Generation and recombination processes via acoustic phonons in disordered graphene

F. T. Vasko* and V. V. Mitin

Department of Electrical Engineering, University at Buffalo, Buffalo, New York 14260-1920, USA

(Received 13 July 2011; revised manuscript received 26 August 2011; published 31 October 2011)

Generation-recombination interband transitions via acoustic phonons are allowed in a disordered graphene because of violation of the energy-momentum conservation requirements. The generation-recombination processes are analyzed for the case of scattering by a static disorder and the deformation interaction of carriers with in-plane acoustic modes. The generation-recombination rates were calculated for the cases of intrinsic and heavily-doped graphene at room temperature. The transient evolution of nonequilibrium carriers is described by the exponential fit dependent on doping conditions and disorder level. The characteristic relaxation times are estimated to be about 150–400 ns for a sample with the maximal sheet resistance of ∼5 kΩ. This rate is comparable with the generation-recombination processes induced by the thermal radiation.

DOI: 10.1103/PhysRevB.84.155445 PACS number(s): 72.80.Vp, 73.63.−b, 78.60.−b

I. INTRODUCTION

Transport[1] and optical[2] properties of graphene as well as noise phenomena in this material[3] are not completely understood for the regime of nonlinear response. The treatment of nonequilibrium carriers requires not only verification of the momentum and energy relaxation processes, but also understanding of the interband generation-recombination processes that determine electron and hole concentrations far from equilibrium (similar transport conditions take place for the bulk gapless materials; see review[4] and references therein). Effective interband transitions via optical phonons of energy $\hbar\omega_0$ take place for the energy of carriers greater than $\hbar\omega_0/2$; see Refs. 5 and 6 where the cases of optical excitation and heating by dc current were analyzed. At lower energies, the generation-recombination processes become ineffective because the Auger transitions are forbidden due to the symmetry of electron-hole states[7] (compare with Ref. 8). Since the carrier's velocity $v \simeq 10^8$ cm/s exceeds significantly the sound velocity s, the interband transitions via acoustic phonons are also forbidden due to the momentum-energy conservation laws. Only slow generation-recombination processes induced by the thermal radiation are allowed in a perfect graphene.[11] To the best of our knowledge, consideration of a disorder effect on the interband transitions via acoustic phonons in the low-energy region, $\varepsilon < \hbar\omega_0/2$, is not performed yet. Thus the evaluation of the generation-recombination rate caused by the interaction of carriers with the acoustic phonon thermostat under violation of the momentum-energy laws in a disordered graphene (allowed electron-hole transitions are depicted in Fig. 1) is timely now.

In this paper, the calculations are performed for the model of short-range disorder whose parameters are taken from the mobility data,[1,10] for samples with the maximal resistance of 2–6 kΩ per square. The probability of electron-hole transitions is expressed through the averaged spectral density functions and is calculated taking into account the contribution of interband interference. Due to slowness of the interband transitions, the quasiequilibrium distributions of electrons and holes with the same temperature are used for the description of a temporal evolution of nonequilibrium concentrations of carriers. The electron and hole concentrations are also connected through the electroneutrality condition with the surface charge controlled by a gate voltage.

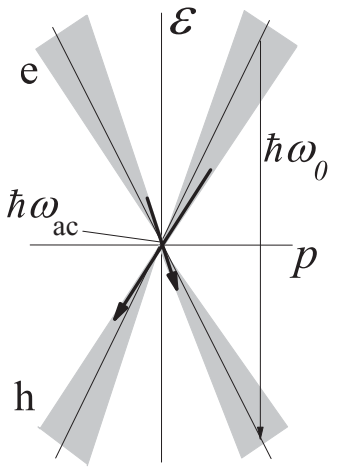

FIG. 1. Interband generation-recombination transitions via acoustic phonons with energies $\sim\hbar\omega_{ac}$ (thick arrows) between broadened electron-hole (e-h, shown by gray) states in the low-energy region, $\varepsilon < \hbar\omega_0/2$. Thin lines show the ideal dispersion law.

The results were obtained for the cases of intrinsic and heavily-doped graphene at temperature T and can be briefly summarized as follows. The concentration balance equation is written through the chemical potential normalized to T and the characteristic rate, which is proportional to a carrier-phonon coupling and increases with temperature as T^2. The transient evolution of nonequilibruim population can be fitted by an exponential decay with the relaxation time 150–400 ns at room temperature and a typical disorder level corresponding to the maximal sheet resistance ∼5 kΩ. This time scale appears to be comparable to the recombination rate via thermal radiation and the mechanism under consideration can be verified by temperature and temporal measurements.

The paper is organized as follows. In the next section, we present the basic equations which describe the generation-recombination processes under consideration. In Sec. III, we evaluate the generation-recombination rates and analyze their dependencies on temperature, disorder level, and doping conditions. The last section includes the discussion of the approximations used and conclusions. In the Appendix, we

consider the generation-recombination mechanism caused by the interaction with the thermal radiation.

II. BASIC EQUATIONS

Temporal evolution of carriers in a random potential, which are weakly interacting with the acoustic phonon modes, is described by the distribution $f_{\alpha t}$ over the states $|\alpha)$ with energies ε_α. An exact with respect to a disorder effect kinetic equation takes the form[11]

$$\frac{\partial f_{\alpha t}}{\partial t} = \sum_{\alpha'} [W_{\alpha'\alpha} f_{\alpha' t}(1 - f_{\alpha t}) - W_{\alpha\alpha'} f_{\alpha t}(1 - f_{\alpha' t})]. \quad (1)$$

The transition probability $W_{\alpha\alpha'}$ is written within the Born approximation with respect to the carrier-phonon interaction with qth phonon mode of frequency ω_q:

$$W_{\alpha\alpha'} = \frac{2\pi}{\hbar} \sum_q |(\alpha|\hat{\chi}_q|\alpha')|^2 [(N_q + 1)\delta(\varepsilon_\alpha - \varepsilon_{\alpha'} - \hbar\omega_q) + N_q \delta(\varepsilon_\alpha - \varepsilon_{\alpha'} + \hbar\omega_q)]. \quad (2)$$

Here the operator $\hat{\chi}_q$ determines the carrier-phonon interaction $\sum_q (\hat{\chi}_q \hat{b}_q + \text{H.c.})$, where $\hat{b}_q$ is the annihilation operator of qth mode and N_q is the Planck distribution of phonons at the equilibrium temperature T. Note that the transition probabilities $W_{\alpha'\alpha}$ and $W_{\alpha\alpha'}$ are connected by $W_{\alpha'\alpha} = \exp[-(\varepsilon_\alpha - \varepsilon_{\alpha'})/T] W_{\alpha\alpha'}$ and

$$\sum_{\alpha\alpha'} [W_{\alpha'\alpha} f_{\alpha' t}(1 - f_{\alpha t}) - W_{\alpha\alpha'} f_{\alpha t}(1 - f_{\alpha' t})] = 0 \quad (3)$$

due to the particle conservation law.

The concentrations of electrons and holes, n_t and $\overline{n}_t$, which are averaged over random disorder (such averaging is denoted as $\langle \cdots \rangle$), are given by

$$\left| \begin{matrix} n_t \\ \overline{n}_t \end{matrix} \right| = \frac{4}{L^2} \left\langle \sum_\alpha \left| \begin{matrix} \theta(\varepsilon_\alpha) f_{\alpha t} \\ \theta(-\varepsilon_\alpha)(1 - f_{\alpha t}) \end{matrix} \right| \right\rangle, \quad (4)$$

where L^2 is the normalization area and the step function $\theta(\pm\varepsilon)$ appears due to the symmetry of the electron-hole spectrum [see Eq. (10) below]. Since effective intraband scattering is caused by the phonon thermostat and carrier-carrier interaction, the quasiequilibrium distributions over the conduction and valence bands are imposed during short-time scales and below we use

$$\tilde{f}_{\varepsilon t} = \begin{cases} \left[\exp\left(\frac{\varepsilon - \mu_t^>}{T}\right) + 1\right]^{-1}, & \varepsilon > 0, \\ \left[\exp\left(\frac{\varepsilon - \mu_t^<}{T}\right) + 1\right]^{-1}, & \varepsilon < 0. \end{cases} \quad (5)$$

Due to effective energy relaxation, the same temperatures are established in both bands. At the same time, the electron and hole concentrations are determined through the different chemical potentials, $\mu_t^>$ and $\mu_t^<$, respectively. The chemical potentials are connected by the electroneutrality condition $n_t - \overline{n}_t = n_s$, where the surface charge en_s is controlled by the gate voltage, V_g, according to $n_s = aV_g$ with $a \simeq 7.2 \times 10^{10}\ \text{cm}^{-2}/\text{V}$ written for the SiO_2 substrate of thickness $0.3\ \mu\text{m}$.

The concentration of electrons is governed by the balance equation $dn_t/dt = (dn/dt)_{\text{ac}}$ with the generation-recombination rate

$$\left(\frac{dn}{dt}\right)_{\text{ac}} = \int_0^\infty d\varepsilon \int_{-\infty}^0 d\varepsilon' W(\varepsilon,\varepsilon') \times \left[\exp\left(\frac{\varepsilon' - \varepsilon}{T}\right)(1 - \tilde{f}_{\varepsilon t})\tilde{f}_{\varepsilon' t} - (1 - \tilde{f}_{\varepsilon' t})\tilde{f}_{\varepsilon t}\right]. \quad (6)$$

We take into account that the intraband transitions (when $\varepsilon, \varepsilon' > 0$) vanish in Eq. (6) and transform the transition probability as follows:

$$W(\varepsilon,\varepsilon') = \frac{4}{L^2} \left\langle \sum_{\alpha\alpha'} \delta(\varepsilon - \varepsilon_\alpha)\delta(\varepsilon' - \varepsilon_{\alpha'}) W_{\alpha\alpha'} \right\rangle. \quad (7)$$

Further, we introduce the exact spectral density function

$$A_\varepsilon(l\mathbf{x}, l'\mathbf{x}') = \sum_\alpha \delta(\varepsilon - \varepsilon_\alpha) \Psi_{l\mathbf{x}}^{(\alpha)} \Psi_{l'\mathbf{x}'}^{(\alpha)*}, \quad (8)$$

which is determined through the double-row wave function $\Psi_{l\mathbf{x}}^{(\alpha)}$ with $l = 1,2$. The column $\Psi_{\mathbf{x}}^{(\alpha)}$ is a solution of the eigenvalue problem $(\hat{h} + V_{\mathbf{x}})\Psi_{\mathbf{x}}^{(\alpha)} = \varepsilon_\alpha \Psi_{\mathbf{x}}^{(\alpha)}$ written through the single-particle Hamiltonian $\hat{h}$ and a random potential $V_{\mathbf{x}}$. Using the definition (2), one obtains the probability $W(\varepsilon,\varepsilon')$ as follows:

$$W(\varepsilon,\varepsilon') = \frac{8\pi}{\hbar L^2} \sum_{\mathbf{q}} |C_q|^2 (N_q + 1)\, \delta(\varepsilon - \varepsilon' - \hbar\omega_q) \times \int d\mathbf{x} \int d\mathbf{x}' e^{i\mathbf{q}\cdot(\mathbf{x} - \mathbf{x}')} \text{tr} \langle \hat{A}_{\varepsilon'}(\mathbf{x},\mathbf{x}') \hat{A}_\varepsilon(\mathbf{x}',\mathbf{x}) \rangle, \quad (9)$$

where $\mathbf{q}$ is the in-plane wave vector and $|C_q|^2$ is the matrix element of deformation interaction.[10] As a result, $(dn/dt)_{\text{ac}}$ is expressed through the electron-hole correlation function with $\varepsilon > 0$ and $\varepsilon' < 0$. Since the main contributions to Eq. (6) appear from energy transfers, $\varepsilon - \varepsilon'$, which exceed the broadening energy, the vertex corrections give a weak contribution to $\langle \hat{A}_{\varepsilon'} \hat{A}_\varepsilon \rangle$. Thus the correlation function can be factorized according to $\langle \hat{A}_{\varepsilon'}(\mathbf{x},\mathbf{x}') \hat{A}_\varepsilon(\mathbf{x}',\mathbf{x}) \rangle \approx \hat{A}_{\varepsilon',\Delta\mathbf{x}} \hat{A}_{\varepsilon,-\Delta\mathbf{x}}$, where $\hat{A}_{\varepsilon,\Delta\mathbf{x}} = \langle \hat{A}_\varepsilon(\mathbf{x},\mathbf{x}') \rangle$ is the averaged spectral function given by the 2×2 matrix.

Below, we calculate the probability (9) using the model of disorder described by the Gaussian correlator $\langle V_{\mathbf{x}} V_{\mathbf{x}'} \rangle = \bar{V}^2 \exp[-(\mathbf{x} - \mathbf{x}')^2/2l_c^2]$, where $\bar{V}$ is the averaged amplitude, l_c is the correlation length, and the cutoff energy $E_c = \upsilon\hbar/l_c$ exceeds the energy scale under consideration. For the low-energy region, $|\varepsilon| \ll E_c$, the model gives $\propto \varepsilon$ relaxation rate, i.e., we deal with a short-range scattering. According to Refs. 12 and 13, the retarded Green's function in the momentum representation takes form:

$$\hat{G}_{\varepsilon,\mathbf{p}}^R = \hat{P}_{\mathbf{p}}^{(+)} G_{\varepsilon,p} + \hat{P}_{\mathbf{p}}^{(-)} G_{\varepsilon,-p}, \quad G_{\varepsilon,p} \approx [\varepsilon(1 + \Lambda_\varepsilon + ig) - \upsilon p]^{-1}, \quad \Lambda_\varepsilon = \frac{g}{\pi} \ln\left(\frac{E_c}{|\varepsilon|}\right), \quad (10)$$

where $\hat{P}_{\mathbf{p}}^{(\pm)} = [1 \pm (\hat{\boldsymbol{\sigma}} \cdot \mathbf{p})/p]/2$ are the projection operators on the conduction (+) and valence (−) bands, $\hat{\boldsymbol{\sigma}}$ is the isospin Pauli matrix, and $g = (\bar{V}^2 l_c/\hbar\upsilon)^2 \pi/2$ is the coupling constant.

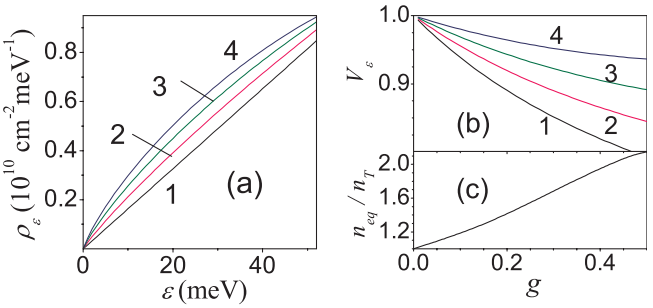

FIG. 2. (Color online) (a) Density of states ρ_ε vs energy at $g = 0$ (1), 0.15 (2), 0.3 (3), and 0.45 (4). (b) Ratio $V_\varepsilon = \sqrt{\overline{\rho}_\varepsilon/\rho_\varepsilon}$ vs g for $\varepsilon = 20$ meV (1), 30 meV (2), 40 meV (3), and 50 meV (4). (c) Equilibrium concentration of nondoped graphene $n_{\rm eq}$ vs g normalized to $n_T \simeq 0.52(T/\hbar\upsilon)^2$.

Here we restrict ourselves by the Born approximation when the self-energy contribution $\varepsilon(\Lambda_\varepsilon + ig)$ is written through the logarithmically-divergent real correction and the damping factor. Note that these corrections vanish at $\varepsilon \to 0$. From a comparision with the mobility data[1,10] one obtains that the parameters $g \simeq 0.45$, 0.3, and 0.15 correspond to the sheet resistances $\sim$6, $\sim$4, and $\sim$2 kΩ per square, respectively. The density of states, $\rho_\varepsilon = -4\,\mathrm{Im}\sum_{\mathbf{p}} \mathrm{tr}\hat{G}^R_{\varepsilon,\mathbf{p}}$, is shown in Fig. 2(a) and $\rho_\varepsilon = \rho_{-\varepsilon}$, i.e., the electron-hole symmetry is not violated due to disorder. Since ρ_ε increases in comparison to the ideal case, $\overline{\rho}_\varepsilon = 2|\varepsilon|/[(\hbar\upsilon)^2\pi]$, the energy-dependent renormalized velocity, υV_ε, decreases up to 10% if $g \leqslant 0.5$ and the concentration of carriers in an intrinsic graphene increases up to two times; see Figs. 2(b) and 2(c), respectively (here $n_T \simeq 8.1 \times 10^{10}$ cm^{-2} is the equilibrium concentration at room temperature and at $g \to 0$).

Furthermore, we use the standard relation $\hat{A}_{\varepsilon,\mathbf{p}} = i(\hat{G}^R_{\varepsilon,\mathbf{p}} - \hat{G}^{R+}_{\varepsilon,\mathbf{p}})/2\pi$ and transform the probability (9) taking into account the energy conservation law:

$$W(\varepsilon,\varepsilon') \approx \{|C_q|^2(N_q+1)\}_{\hbar\omega_q=\varepsilon-\varepsilon'} \times \frac{8\pi}{\hbar L^2}\sum_{\mathbf{pp}'}\delta(\varepsilon-\varepsilon'-s|\mathbf{p}-\mathbf{p}'|)\mathrm{tr}(\hat{A}_{\varepsilon',\mathbf{p}'}\hat{A}_{\varepsilon,\mathbf{p}}). \tag{11}$$

The trace here should be taken using $\mathrm{tr}(\hat{P}^{(\pm)}_{\mathbf{p}'}\hat{P}^{(\pm)}_{\mathbf{p}}) = [1 + (\mathbf{p}\cdot\mathbf{p}')/pp']/2$ and $\mathrm{tr}(\hat{P}^{(\pm)}_{\mathbf{p}'}\hat{P}^{(\mp)}_{\mathbf{p}}) = [1 - (\mathbf{p}\cdot\mathbf{p}')/pp']/2$. This result differs from the standard consideration,[14] because interference of electron and hole states gives an essential contribution to $W(\varepsilon,\varepsilon')$ due to the matrix structure of the spectral density functions. After the integrations over $\mathbf{p}$ plane, one transforms Eq. (11) into

$$W(\varepsilon,\varepsilon') \equiv \Theta_{\rm GR} w(\varepsilon/T, -\varepsilon'/T)/T^2,$$
$$\Theta_{\rm GR} = \frac{\upsilon_{\rm ac} s}{\upsilon^2}\frac{T}{\hbar}\left(\frac{T}{\pi\hbar\upsilon}\right)^2, \quad \upsilon_{\rm ac} = \frac{D^2 T}{4\hbar^2\rho_s \upsilon s^2}, \tag{12}$$

where we separated the dimensionless kernel, $w(\xi,\xi')$, and the factor, $\Theta_{\rm GR}$, which is written for the case of the deformation interaction of carriers with the in-plane acoustic modes; see Refs. 10 and 13. Here D is the deformation potential, s is the sound velocity, and ρ_s is the sheet density of graphene. At room

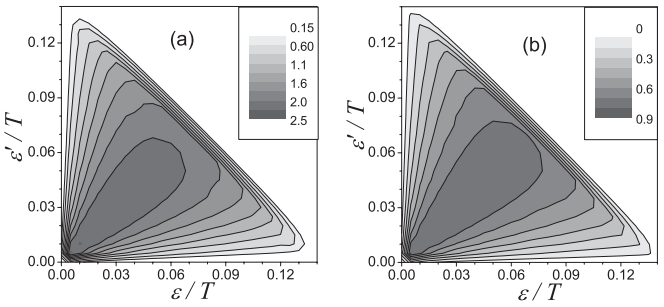

FIG. 3. Contour plots of dimensionless kernels $w(\varepsilon/T,\varepsilon'/T)$ for $g = 0.4$ (a) and $g = 0.2$ (b).

temperature and typical other parameters,[10] we obtain $\upsilon_{\rm ac} \simeq 0.96 \times 10^6$ cm/s and $\Theta_{\rm GR} \simeq 5.06 \times 10^{19}$ cm^{-2}s^{-1} (notice that $\upsilon_{\rm ac} \propto D^2$ and we used $D \simeq 12$ eV). The dimensionless kernel is plotted in Fig. 3 and the probability $W(\varepsilon,\varepsilon')$ is suppressed fast if $(\varepsilon - \varepsilon')/T \geqslant 0.15$. This cutoff factor is determined by the weak ratio $s/\upsilon \simeq 1/137$ mainly while parameter g determines a peak value of $W(\varepsilon,\varepsilon')$; cf. Figs. 3(a) and 3(b).

The generation-recombination rate (6) is written through Eqs. (11) and (12) with the use of the dimensionless variables $\xi = \varepsilon/T$ and $\xi' = \varepsilon'/T$:

$$\left(\frac{dn}{dt}\right)_{\rm ac} = \Theta_{\rm GR}\int_0^\infty d\xi\int_0^\infty d\xi' w(\xi,\xi') \times \frac{e^{-\xi'-\mu_t^>/T} - e^{-\xi'-\mu_t^</T}}{\left[\exp\left(\xi - \frac{\mu_t^>}{T}\right)+1\right]\left[\exp\left(\xi' - \frac{\mu_t^<}{T}\right)+1\right]} \tag{13}$$

For typical concentrations of carriers, $\mu_t^<$ and $\mu_t^>$ exceed $0.15T$ and one can simplify the rate as follows:

$$\left(\frac{dn}{dt}\right)_{\rm ac} \approx \Theta_{\rm GR}\frac{w_g\left[e^{-\mu_t^>/T} - e^{-\mu_t^</T}\right]}{\left[e^{-\mu_t^>/T}+1\right]\left[e^{-\mu_t^</T}+1\right]}, \quad w_g = \int_0^\infty d\xi\int_0^\infty d\xi' w(\xi,\xi'), \tag{14}$$

where the averaged over energies kernel w_g is plotted versus g in Fig. 4, together with a simple quadratic fit. For the disorder level corresponding to the resistance $\sim$5 kΩ per square, one obtains $w_g \simeq 0.02$.

III. RESULTS

In this section, we analyze the concentration balance equation $dn_t/dt = (dn/dt)_{\rm ac}$, where the right-hand side is given by Eq. (14) and is written through $\psi_t^> = \mu_t^>/T$ and

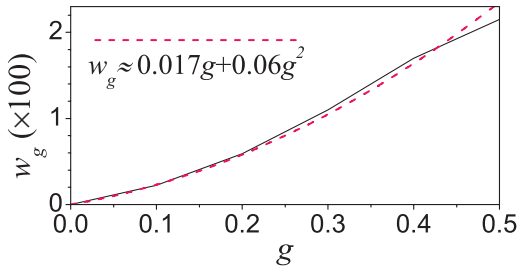

FIG. 4. (Color online) Averaged kernel w_g vs coupling constant g. Dashed curve corresponds to the quadratic fit.

$\psi_t^< = \mu_t^>/T$. The initial conditions $\psi_{t=0}^> = \psi_0^>$ and $\psi_{t=0}^< = \psi_0^<$ are determined through the initial concentrations $n_{t=0}$ and $\overline{n}_{t=0}$ according to Eq. (4). Variables $\psi_t^>$ and $\psi_t^<$ are connected through the electroneutrality condition,

$$\int_0^\infty d\varepsilon\, \rho_\varepsilon \left(\frac{1}{e^{\varepsilon/T-\psi_t^>}+1} - \frac{1}{e^{\varepsilon/T+\psi_t^<}+1} \right) = n_s, \quad (15)$$

and below we consider the limiting cases of an intrinsic graphene ($n_s = 0$) and a n-type heavily-doped graphene ($n_s > 0$). Since a slowness of generation-recombination processes in comparison to the intraband relaxation, any kinetic phenomenon can be considered with the use of concentrations which are parametrically dependent on time.

A. Intrinsic graphene

For the case under consideration, $\psi_t^> = -\psi_t^< \equiv \psi_t$ and the concentration of electrons (or holes, because now $n_t = \overline{n}_t$) is given by $n_t = \int_0^\infty d\varepsilon\, \rho_\varepsilon [\exp(\varepsilon/T - \psi_t) + 1]^{-1}$, so that n_t and ψ_t are connected through

$$\frac{dn_t}{dt} = \frac{d\psi_t}{dt} \int_0^\infty \frac{d\varepsilon\, \rho_\varepsilon}{1+\cosh(\varepsilon/T-\psi_t)} \quad (16)$$

and the concentration balance equation is derived from Eq. (13) as

$$\frac{dn_t}{dt} = -\Theta_{\rm GR} w_g \tanh\left(\frac{\psi_t}{2}\right). \quad (17)$$

As a result, Eqs. (16) and (17) are transformed into the first-order differential equation for ψ_t with the initial condition $\psi_{t=0} = \psi_0$, where ψ_0 is determined through the $n_{t=0}$. The implicit solution of this equation takes form

$$\nu_{\rm GR} t = \int_{\psi_t}^{\psi_0} d\psi\, F(\psi), \quad \nu_{\rm GR} = w_g \frac{\upsilon_{\rm ac} s}{\pi \upsilon^2} \frac{T}{\hbar},$$
$$F(\psi) = \tanh\left(\frac{\psi}{2}\right) \int_0^\infty \frac{d\xi\, r_\xi}{1+\cosh(\xi-\psi)}. \quad (18)$$

Here $r_\xi = \rho_{\xi T}/\overline{\rho}_T$ is the dimensionless density of states and the temporal evolution of n_t is described through the characteristic rate $\nu_{\rm GR}$ and the dimensionless function $F(\psi)$. At room temperature and at $w_g \simeq 0.02$, one obtains $\nu_{\rm GR} \simeq 1.85 \times 10^7$ s^{-1} for the parameters used; $\nu_{\rm GR}$ increases with T and with disorder level because $\nu_{\rm GR} \propto w_g T$. Since $\nu_{\rm GR} \propto D^2$, the rate increases up to 10^8 s^{-1}, if $D \sim 20$ eV, as it was measured in Ref. 15 (note that a lower D was also reported recently[16]).

Figure 5 shows the transient evolution of n_t from the initial concentration $n_{t=0}$ to the equilibrium concentration $n_{\rm eq}$, which is determined by $n_{\rm eq} = \int_0^\infty d\varepsilon\, \rho_\varepsilon [\exp(\varepsilon/T) + 1]^{-1}$, taking into account the disorder-induced renormalization of ρ_ε; see Fig. 2. We plotted n_t for the cases of recombination or generation of carriers, if $n_{t=0} > n_{\rm eq}$ or $n_{t=0} < n_{\rm eq}$, respectively. The relaxation becomes suppressed if the disorder level decreases both due to a slowness of dependency on $\nu_{\rm GR} t$, compare curves for $g = 0.5$ and 0.25 in Fig. 5, and, mainly, due to the relation $\nu_{\rm GR} \propto w_g$; see Fig. 4. Within a 5% accuracy, the evolution of n_t can be fitted by the exponential dependence

$$n_t \approx n_0 + n_{\rm eq}[1 - \exp(-\alpha \nu_{\rm GR} t)], \quad (19)$$

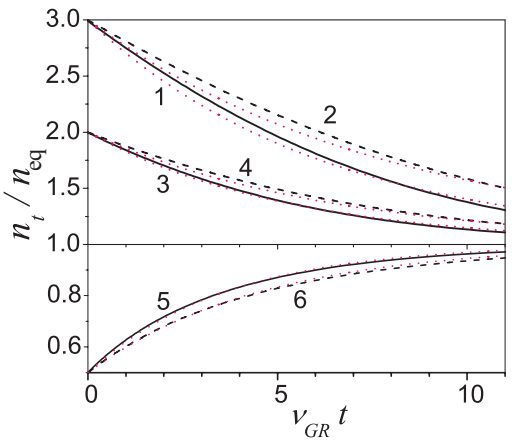

FIG. 5. (Color online) Transient evolution of concentration n_t at different initial conditions: $n_{t=0} = 3n_{\rm eq}$ (1,2), $n_{t=0} = 2n_{\rm eq}$, (3,4), and $n_{t=0} = 0.5n_{\rm eq}$ (5,6) for coupling parameters $g = 0.25$ (1, 3, 5) and $g = 0.5$ (2, 4, 6). Dotted curves correspond to exponential fits (19), with $\alpha = 0.16$ (1), 0.125 (2), 0.19 (3), 0.155 (4), 0.22 (5), and 0.275 (6).

with the parameter α varying between 0.16 and 0.28 depending on initial condition and on disorder level (the numerical data are given in the figure caption). This parameter slightly increases if disorder level decreases for $n_{t=0} > n_{\rm eq}$ and the generation process is faster than the recombination one. The corresponding times, $(\alpha \nu_{\rm GR})^{-1}$, equal 338 ns (1), 284 ns (3), and 196 ns (5) for $g \simeq 0.25$. For $g \simeq 0.5$ (curves 2, 4, and 6), these times vary between 310 and 180 ns. Such a time scale is comparable to the radiative recombination times, see the Appendix, so that the contribution under consideration can be extracted due to different temperature dependencies.

B. Heavily-doped graphene

We turn now to the case of a heavily-doped graphene, when $\psi_t^> \gg 1$ and it is convenient to introduce a weak variation $\delta\psi_t = \psi_t^> - \psi_s$, where ψ_s corresponds to the equilibrium case with concentration n_s. Neglecting a hole concentration and using the step-like Fermi function in c-band, one obtains n_s from Eq. (15):

$$n_s \approx \int_0^{\psi_s T} d\varepsilon\, \rho_\varepsilon. \quad (20)$$

As a result, $\delta\psi_t$ and $\psi_t^<$ are connected by the electroneutrality condition (15) as follows:

$$\delta\psi_t \approx \frac{\overline{\rho}_T}{\rho_{\varepsilon=\psi_s T}} \int_0^\infty \frac{d\xi\, r_\xi}{1+\exp(\xi+\psi_t^<)}, \quad (21)$$

where the ratio $\overline{\rho}_T/\rho_{\varepsilon=\psi_s T}$ can be found from Fig. 2(a). Using Eq. (14), we transform the concentration balance equation into the form

$$\frac{d\delta\psi_t}{dt} = -\frac{\nu_{\rm GR}\overline{\rho}_T}{2\rho_{\varepsilon=\psi_s T}[1+\exp(\psi_t^<)]}. \quad (22)$$

Substituting the relation (21) into Eq. (22), one obtains the first-order differential equation for $\psi_t^<$, with the implicit solution

$$\nu_{\rm GR} t = \int_{\overline{\psi}_0}^{\psi_t^<} d\psi \int_0^\infty \frac{d\xi\, r_\xi (1+e^\psi)}{1+\cosh(\xi+\psi)}, \qquad (23)$$

where $\overline{\psi}_0 = \psi_{t=0}^<$ appears from the initial condition. Notice that the factor $\overline{\rho}_T/\rho_{\varepsilon=\psi_s T}$ drops out from the solution (23), i.e., the transient process under consideration does not depend on the doping level because the only low-energy states are involved in the interband transitions.

Furthermore, we plot the transient evolution of the hole concentration $\overline{n}_t = n_t - n_s$ determined through $\psi_t^<$ according to $\overline{n}_t = \int_0^\infty d\varepsilon\, \rho_\varepsilon [\exp(\varepsilon/T + \psi_t^<) + 1]^{-1}$. Figure 6 shows the concentration $\overline{n}_t$ versus dimensionless time, $\nu_{\rm GR} t$, for the initial conditions written through the characteristic concentration n_T; see Fig. 2. Similarly to the undoped case, the exponential fits $(n_t - n_s)/(n_{t=0} - n_s) \approx \exp(-\beta \nu_{\rm GR} t)$ with $\beta \simeq 0.12$ (1), 0.15 (2), and 0.2 (3) describe the transient evolution with an accuracy of ~10% if $\nu_{\rm GR} t < 10$. An enhancement of recombination takes place at tails of transient evolution, if $\nu_{\rm GR} t > 10$. Since the relaxation rate increases with the disorder level because $\nu_{\rm GR} \propto w_g$ (in spite of β decreasing slightly with disorder level), the recombination process becomes faster in spite of an opposite dependency on $\nu_{\rm GR} t$ in Fig. 6. The relaxation times, $\sim(\beta \nu_{\rm GR})^{-1}$, equal 450 ns (1), 360 ns (2), and 270 ns (3) for $g = 0.25$ and different initial conditions. For $g = 0.5$, these times vary between 410 and 240 ns. Once again, the recombination scale is comparable to the radiative recombination process shown in Fig. 7(b); see the Appendix. The time scales obtained should be changed by a factor of 0.2–4 depending on the value of the deformation potential used.[15,16]

IV. SUMMARY AND CONCLUSIONS

We have examined the new channel for interband generation-recombination process of carriers in a disordered graphene via acoustic phonons. The efficiency of transitions increases with disorder level and concentration of nonequilibrium carriers as well as with temperature. We have found that

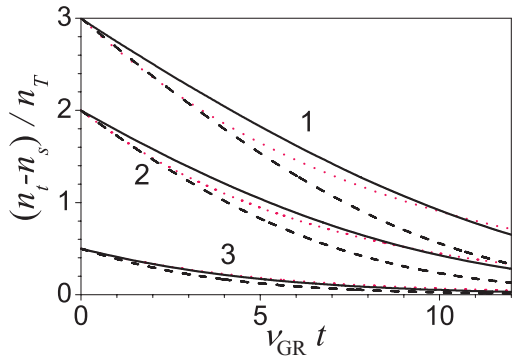

FIG. 6. (Color online) Transient evolution of hole concentration $n_t - n_s$ at different initial conditions: $n_{t=0} - n_s = 3n_T$ (1), $n_{t=0} - n_s = 2n_T$ (2), and $n_{t=0} - n_s = 0.5n_T$ (3). Solid and dashed curves correspond to coupling parameters $g = 0.5$ and $g = 0.25$, respectively. Dotted curves correspond to the exponential fits.

the relaxation rate belongs to a submicrosecond range for the samples with typical disorder level at room temperature.

Let us discuss the assumptions used in the presented calculations. The main restriction of the results is the description of the response in the framework of the quasiequilibrium approach, with different chemical potentials in c- and v-bands but the same temperature due to the fast energy relaxation caused by phonon and carrier-carrier scattering processes. We also restrict ourselves by the phenomenological model of the disorder scattering.[11] Since a low-energy region is only essential in $W(\varepsilon,\varepsilon')$ and the results are written through the kernel (14), a microscopic mechanism of elastic relaxation (which remains under debate up to now[1,17]) is not important for the process under consideration. By analogy with the description of transport phenomena,[1,10,12] more complicated calculations for finite-range disorder should give similar results. However, the case of impurities with a low-energy resonant level, which was discussed recently in Refs. 18, requires a special consideration. Besides this, the Coulomb renormalization of υ leads to a weak modification of the transition probability (12). We considered the deformation interaction of carriers with longitudinal acoustic modes[10,13] neglecting scattering by surface phonons of the substrate in agreement with the experimental data.[19] Such a contribution can only restrict the energies under consideration because of the lower surface phonon energy (~55 meV for the SiO_2 substrate). Since the nondiagonal components give a weak contribution to the concentration balance equation under consideration,[11] we take into account only diagonal components of the density matrix $f_{\alpha t}$ while evaluating of the generation-recombination rate. The simplifications mentioned above do not change either the peculiarities of the generation-recombination processes or the numerical estimates of relaxation times given in Sec. III.

Next, we briefly consider some possibilities for experimental verification of the mechanism of interband transitions suggested. It is clear from a comparison of the results in Sec. III and in the Appendix that interband transitions via acoustic phonons and via thermal radiation can be separated due to different temperature and concentration dependencies of damping. A possible contribution of the disorder-induced Auger process is weak for a low concentration of nonequilibrium carriers and temperature dependencies should be different. This contribution is beyond our consideration and requires a special study. In contrast to the ultrafast optical measurements applied for the study of the relaxation and recombination of high-energy carriers,[2] a transient evolution of concentration over time scales ~100 ns can be measured directly (e.g., in Ref. 6 the transient response under abrupt switching on of a dc field lasts up to hundreds of nanoseconds). However, under a verification of the slow process examined, a possible contact injection or a trapping into substrate states should be analyzed.

To conclude, we believe that the generation-recombination via acoustic phonons can be verified experimentally and more detailed numerical calculations are necessary in order to separate this mechanism from other contributions. The results obtained will stimulate a further study of the generation-recombination processes that are essential in many transport and optical phenomena far from equilibrium.

ACKNOWLEDGMENT

This paper is based upon work supported by the National Science Foundation under Grant No. DMR 0907126.

APPENDIX: RADIATIVE TRANSITIONS

Below we describe the generation-recombination processes that are associated with the interband transitions induced by the thermal radiation and evaluate the radiative relaxation rate for the weak disorder case, $g \ll 1$. The corresponding collision integral was evaluated in Ref. 9 and the kinetic equation for the electron distribution f_{ept} takes the form

$$\frac{\partial f_{ept}}{\partial t} = \nu_p^{(R)}[N_{2\upsilon p/T}(1 - f_{ept} - f_{hpt}) - f_{ept} f_{hpt}], \qquad \text{(A1)}$$

where $N_{2\upsilon p/T}$ describes the Planck distribution of the thermal photons at temperature T. The hole distribution can be obtained from the condition $\partial(f_{ept} + f_{hpt})/\partial t = 0$. The interband absorption or emission of photons are described by the first or second terms in the right-hand side of Eq. (A1) and are responsible for the generation or recombination processes. The rate of spontaneous radiative transitions is given by $\nu_p^{(R)} = \upsilon_R p/\hbar$, where we have introduced the characteristic velocity $\upsilon_R \simeq 41.6$ cm/s for graphene surrounded by SiO_2 layers. Similar to Eq. (6), contribution of the radiative collision integral from Eq. (A1) into the concentration balance equation takes the form $(dn/dt)_{\rm ac} = (4/L^2)\sum_{\mathbf{p}} \nu_p^{(R)}[N_{2\upsilon p/T}(1 - f_{ept} - f_{hpt}) - f_{ept} f_{hpt}]$.

For the case of an intrinsic graphene, the balance equation is written by analogy with Sec. III A through $\psi_t = \mu_t/T$:

$$\frac{d\psi_t}{dt} = -\nu_R \frac{F_i(\psi_t)}{N(\psi_t)}, \quad \nu_R = \frac{2\upsilon_R}{\upsilon}\frac{T}{\hbar}, \qquad \text{(A2)}$$

where $\nu_R^{-1} \approx 30$ ns is the radiative recombination time at room temperature. The functions $F_i(\psi)$ and $N(\psi)$ are given by

$$F_i(\psi) = \int_0^\infty \frac{d\xi\, \xi(1 - e^{-2\psi})}{(1 - e^{-2\xi})(e^{\xi-\psi} + 1)^2}, \qquad N(\psi) = \int_0^\infty \frac{d\xi\, \xi}{1 + \cosh(\xi - \psi)}, \qquad \text{(A3)}$$

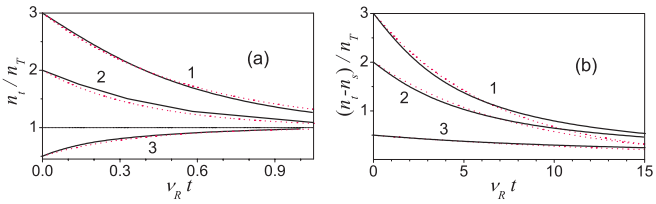

FIG. 7. (Color online) Transient evolution of concentration due to interband radiative transitions for intrinsic (a) and heavily-doped (b) graphene at different initial conditions: $n_{t=0} = 3n_T$ (1), $n_{t=0} = 2n_T$ (2), and $n_{t=0} = 0.5n_T$ (3). Dotted curves correspond to exponential fits.

and the implicit solution of Eqs. (A2) and (A3) is given by the formula similar to Eq. (18):

$$\nu_R t = \int_{\psi_0}^{\psi_t} d\psi \frac{N(\psi)}{F_i(\psi)}. \qquad \text{(A4)}$$

In Fig. 7(a), we plot the transient evolution of concentration versus the dimensionless time, $\nu_R t$, for the same initial conditions as in Fig. 5. These transient dependencies are described by the exponential decay given by Eq. (19) with $\alpha \approx 0.25$ for all cases. Thus one obtains the radiative recombination time $\sim 4/\nu_R \approx 120$ ns, which does not depend on an initial concentration.

For the case of doped graphene, the concentration balance equation (22) should be replaced by

$$\frac{d\delta\psi_t}{dt} = -\frac{\nu_R}{2} F_d(\psi_t^<), \qquad F_d(\psi) = \int_0^\infty \frac{d\xi\, \xi^2}{\left(1 - e^{-2\xi}\right)\left(e^{\xi+\psi} + 1\right)}, \qquad \text{(A5)}$$

while the relation between $\delta\psi_t$ and $\psi_t^<$ takes the form [cf. Eq. (21)]

$$\delta\psi_t \approx \frac{1}{\psi_s}\int_0^\infty \frac{d\xi\, \xi}{1 + \exp(\xi + \psi_t^<)}. \qquad \text{(A6)}$$

As a result, the equation for $\psi_t^<$ has the only difference from Eq. (2) due to the replacement $F_i(\psi)$ by $F_d(\psi)$. The implicit solution of Eqs. (A5) and (A6) is given by Eq. (A4) with the same replacement. In Fig. 7(b), we plot the transient evolution of hole concentration, $\overline{n}_t/n_T$, for the same initial conditions as in Fig. 6. The corresponding exponential fits are determined by the coefficients $\beta \simeq 0.15$ (1), 0.125 (2), and 0.06 (3), i.e., the relaxation rate depends on hole concentration. At room temperature, the radiative recombination time $(\beta\nu_R)^{-1}$ corresponds to the time interval between 190 and 480 ns.

*ftvasko@yahoo.com

[1] N. M. R. Peres, Rev. Mod. Phys. **82**, 2673 (2010).

[2] M. Orlita and M. Potemski, Semicond. Sci. Technol. **25**, 063001 (2010); F. Bonaccorso, Z. Sun, T. Hasan, and A. C. Ferrari, Nature Photon. **4**, 611 (2010).

[3] S. Rumyantsev, G. Liu, W. Stillman, M. Shur, and A. A. Balandin, J. Phys. Condens. Matter **22**, 395302 (2010).

[4] A. V. Germanenko and G. M. Minkov, Phys. Status Solidi B **184**, 9 (1994).

[5] F. Rana, P. A. George, J. H. Strait, J. Dawlaty, S. Shivaraman, M. Chandrashekhar, and M. G. Spencer, Phys. Rev. B **79**, 115447 (2009); F. T. Vasko, *ibid.* **82**, 245422 (2010).

[6] P. N. Romanets and F. T. Vasko, Phys. Rev. B **83**, 205427 (2011).

[7]M. S. Foster and I. L. Aleiner, Phys. Rev. B **79**, 085415 (2009); D. M. Basko, S. Piscanec, and A. C. Ferrari, *ibid.* **80**, 165413 (2009).
[8]F. Rana, J. H. Strait, H. Wang, and C. Manolatou, Phys. Rev. B **84**, 045437 (2011); T. Winzer, A. Knorr, and E. Malic, Nano Lett. **10**, 4839 (2010); F. Rana, Phys. Rev. B **76**, 155431 (2007).
[9]F. T. Vasko and V. Ryzhii, Phys. Rev. B **77**, 195433 (2008).
[10]F. T. Vasko and V. Ryzhii, Phys. Rev. B **76**, 233404 (2007).
[11]F. T. Vasko and O. E. Raichev, *Quantum Kinetic Theory and Applications* (Springer, New York, 2005).
[12]T. Ando, J. Phys. Soc. Jpn. **75**, 074716 (2006); P. M. Ostrovsky, I. V. Gornyi, and A. D. Mirlin, Phys. Rev. B **74**, 235443 (2006).
[13]T. Stauber, N. M. R. Peres, and A. H. Castro Neto, Phys. Rev. B **78**, 085418 (2008).
[14]G. D. Mahan, *Many-Particle Physics* (Plenum, New York, 1990).
[15]K. I. Bolotin, K. J. Sikes, J. Hone, H. L. Stormer, and P. Kim, Phys. Rev. Lett. **101**, 096802 (2008); J.-H. Chen, C. Jang, M. Ishigami, S. Xiao, E. D. Williams, and M. S. Fuhrer, Solid State Commun. **149**, 1080 (2009).
[16]K. M. Borysenko, J. T. Mullen, E. A. Barry, S. Paul, Y. G. Semenov, J. M. Zavada, M. B. Nardelli, and K. W. Kim, Phys. Rev. B **81**, 121412 (2010).
[17]L. A. Ponomarenko, R. Yang, T. M. Mohiuddin, M. I. Katsnelson, K. S. Novoselov, S. V. Morozov, A. A. Zhukov, F. Schedin, E. W. Hill, and A. K. Geim, Phys. Rev. Lett. **102**, 206603 (2009); S. Adam, P. W. Brouwer, and S. Das Sarma, Phys. Rev. B **79**, 201404 (2009).
[18]V. M. Pereira, J. M. B. Lopes dos Santos, and A. H. Castro Neto, Phys. Rev. B **77**, 115109 (2008); B. Dora, K. Ziegler, and P. Thalmeier, *ibid.* **77**, 115422 (2008); M. Titov, P. M. Ostrovsky, I. V. Gornyi, A. Schuessler, and A. D. Mirlin, Phys. Rev. Lett. **104**, 076802 (2010).
[19]A. Barreiro, M. Lazzeri, J. Moser, F. Mauri, and A. Bachtold, Phys. Rev. Lett. **103**, 076601 (2009); S. Fratini and F. Guinea, Phys. Rev. B **77**, 195415 (2008).